Multicenter distorted-wave method for fast-electron-impact single ionization of molecules

Song bin Zhang,[1,2,*] Xing Yu Li,[1] Jian Guo Wang,[3] Yi Zhi Qu,[4] and Xiangjun Chen[1,5,†]

[1]*Hefei National Laboratory for Physical Sciences at Microscale and Department of Modern Physics, University of Science and Technology of China, Hefei 230026, China*

[2]*Max Planck Institute for the Physics of Complex Systems, 01187 Dresden, Germany and Center for Free-Electron Laser Science, 22761 Hamburg, Germany*

[3]*Key Laboratory of Computational Physics, Institute of Applied Physics and Computational Mathematics, P.O. Box 8009, Beijing 100088, China*

[4]*College of Material Sciences and Optoelectronic Technology, University of Chinese Academy of Sciences, P.O. Box 4588, Beijing 100049, China*

[5]*Synergetic Innovation Center of Quantum Information and Quantum Physics, University of Science and Technology of China, Hefei, Anhui 230026, China*

(Received 12 March 2014; published 16 May 2014)

A multicenter distorted-wave (MCDW) method for fast-electron-impact single ionization of a molecular system in the coplanar-asymmetric kinematics is developed. Plane waves are used to describe the fast incoming and outgoing electrons and the multicenter nature of the molecule is considered by describing the slow ejected electron with the multicenter distorted wave, which is solved from the anisotropic multicenter potential between the ejected electron and the ionic molecule. The MCDW method improves the conventional molecular distorted-wave methods, whose distorted wave is solved from the spherically averaged isotropic potential. The application to the water molecule shows reasonable agreement with the available experimental data.

DOI: 10.1103/PhysRevA.89.052711 PACS number(s): 34.80.Gs

I. INTRODUCTION

It is well known that electron-impact single ionization is a fundamental process in atomic and molecular physics. However, a complete understanding of the dynamics is still one of the biggest challenges in atomic and molecular physics. Many experimental and theoretical works have been performed to study this process for atomic and molecular systems [1–7]. When both the incoming and outgoing electrons are fast, the electrons will quickly leave the target and the interactions between the electrons and the target could be neglected and the states of all the free electrons could be well described by the plane waves. McCarthy and co-workers [1,2,4,6] found that, in the plane-wave impulse approximation, the triple-differential cross section (TDCS) for the electron-impact single-ionization process is proportional to the electron density distribution of the atomic or molecular ionized electron orbital (Dyson orbital) in momentum space, which results in the foundation of the well-known electron momentum spectroscopy or binary $(e, 2e)$ spectroscopy [1,4–6].

When the incoming and outgoing electrons are not so fast [8], the interactions between the electrons and the target become important, plane waves cannot well describe the states of the free electrons, and the impact ionization process becomes a pure dynamical process. Different kinds of theoretical methods have been developed for the atomic system, such as the distorted-wave impulse approximation (DWIA) [1,9,10], distorted-wave Born approximation (DWBA) [9–11], Brauner-Briggs-Klar theory [12–14], B-spline R-matrix approach [15,16], convergent close-coupling (CCC) method [17–19], exterior complex scaling (ECS) method [20–22], and time-dependent close-coupling (TDCC) method [23–25]. We note that the ECS, CCC, and TDCC methods could almost exactly solve the three-body system (electron plus hydrogen). However, no general and efficient method has been developed for molecular systems. One big challenge comes from the anisotropic multicenter nature of the molecular system, which means that the free electron will be scattered by the anisotropic multicenter potential. It would be difficult to describe the complex state of the slow free electron, especially in the small-r region, where r indicates the position relative to the center of mass of the molecule.

Nevertheless, there are many progressive theoretical works [7,26–47]. It is worth mentioning that Champion and co-workers [29,46] and Madison and co-workers [7,32–36] have developed atomiclike distorted-wave methods for molecular system; both groups employed the spherically averaged isotropic potentials to describe the distorted waves of the free electrons, while the latter authors also tried the spherically averaged molecular wave function. These methods have successfully described the dynamics of the ionization process for some cases. However, the slow free electron could be strongly scattered by the anisotropic multicenter nature of the molecule and an atomiclike distorted wave may not describe the true state of the slow free electron. Also it should be noted that more advanced *ab initio* calculations (TDCC and CCC) have been performed for some simple diatomic molecules [40–45], but it would be very difficult to extend them to more complex molecules. Therefore, the development of some new methods to study more complex molecules is greatly anticipated and the multicenter distorted-wave (MCDW) method could be one of these. It extends the conventional DWBA method by employing the true anisotropic multicenter potential to calculate the distorted wave for the slow free electron.

The theory is constructed within the coplanar-asymmetric kinematics [6] in this work and the incoming and scattered

*songbin@pks.mpg.de
†xjun@ustc.edu.cn

electrons are fast in the kinematics. These fast electrons can be well described by the plane waves and the ionization dynamics will be sensitive to the ejected slow electron. Coplanar-asymmetric (e,2e) kinematics could provide a good test of the present multicenter method. This paper is organized as follows. The multicenter distorted-wave method for the coplanar-asymmetric kinematics is presented in the next section, followed by the application to H_2O and a comparison with the experimental data [31] in Sec. III. A simple summary is given in Sec. IV. Atomic units are used throughout the paper unless explicitly stated otherwise.

II. THEORETICAL METHOD

A. General formalism

Generally speaking, the electron scattering process is much faster than all the possible rotational and vibrational periods of the molecular system. The closure relation could be applied to these states and only the pure electronic states play a role in the transition matrix. The total observables can be obtained by averaging all the molecular orientations weighted by the density distributions of the rotational wave packet. To simplify the notation, rotational and vibrational states will not be explicitly expressed when describing the states of the molecules.

The molecular orientation is defined by the Euler angles $\Omega = (\alpha,\beta,\gamma)$ and $\Omega = (0,0,0)$ corresponds to the initial or reference molecular orientation. The molecular wave function $\psi_\Omega(\mathbf{r})$ at a given orientation Ω can be obtained by rotating the initial wave function $\psi_{\Omega=0}(\mathbf{r})$ as $\psi_\Omega(\mathbf{r}) = R_\Omega\psi_0(\mathbf{r}) = \psi_0(R_\Omega\mathbf{r})$, where R_Ω is the corresponding Euler rotation operator. The z-y-z convention is employed throughout this work. The nonrelativistic eightfold-differential cross section (8DCS) in the first Born approximation reads [28]

$$\left[\frac{d^8\sigma}{d\Omega_2 d\Omega_1 dE_1 d\alpha d\beta d\gamma}(\alpha,\beta,\gamma)\right] = \frac{1}{(2\pi)^5}\frac{k_1k_2}{k_0}|T_{fi}(\alpha,\beta,\gamma)|^2, \tag{1}$$

where Ω_1 and Ω_2 represent the solid angles of detection for the scattered and the ejected electrons, respectively, and $\mathbf{k}_0$, $\mathbf{k}_1$, and $\mathbf{k}_2$ are, respectively, the momenta for the incoming, scattered, and ejected electrons with the corresponding energies $E_i = k_i^2/2 (i = 0,1,2)$. The transition matrix T_{fi} describes the transition of the total system from the initial state ψ_i to the final state $\psi_f^{(-)}$ through the interaction potential V and is given by

$$T_{fi}(\Omega) = \langle\psi_f^{(-)}(R_\Omega\mathbf{r})|V(\mathbf{r})|\psi_i(R_\Omega\mathbf{r})\rangle. \tag{2}$$

Note that in the coplanar-asymmetric kinematics, the scattered electron is much faster than the ejected electron. Therefore, the exchange effect would be small and is neglected in the above expression. The potential V represents the interaction between the incident electron and the target and can be written as

$$V = -\sum_n \frac{Z_n}{|\mathbf{r}_0 - \mathbf{R}_n|} + \sum_e^{n_e}\frac{1}{|\mathbf{r}_0 - \mathbf{r}_e|}, \tag{3}$$

where $\mathbf{R}_n$ is the position of the nth nucleus with charge Z_n and $\mathbf{r}_0$ and $\mathbf{r}_e$ are the positions for incoming electron and the eth bound electron of the target, respectively.

In the present model, the initial and final states of the total system are described by the product of two wave functions and three wave functions, respectively. The former corresponds to the incoming electron and the molecule, while the latter corresponds to the scattered electron, the ejected electron, and the ionic molecule. Within the frozen-core approximation, the n_e-electron problem can be reduced to a one-active-electron problem. Furthermore, the fast incoming and scattered electrons can be well described by the plane waves, i.e., $\phi_j(\mathbf{k}_j,\mathbf{r}_j) = e^{i\mathbf{k}_j\cdot\mathbf{r}_j}$ $(j = 0,1)$. Employing the Bethe integral

$$\int \frac{e^{i\mathbf{k}\cdot\mathbf{r}'}}{|\mathbf{r} - \mathbf{r}'|}d\mathbf{r}' = \frac{4\pi}{k^2}e^{i\mathbf{k}\cdot\mathbf{r}},$$

the transition matrix element in the laboratory frame can be rewritten as

$$\begin{aligned} T_{if}^s(\Omega) &= \left\langle\phi_1(\mathbf{k}_1,\mathbf{r}_0)\varphi_2^{s(-)}(\mathbf{k}_2,R_\Omega\mathbf{r}_1)\right|\frac{1}{|\mathbf{r}_0 - \mathbf{r}_1|} \\ &\quad - \frac{\sum_n \frac{Z_n}{|\mathbf{r}_0 - \mathbf{R}_n|}}{\sum_n Z_n}\left|\phi_0(\mathbf{k}_0,\mathbf{r}_0)\varphi_i^s(R_\Omega\mathbf{r}_1)\right\rangle \\ &= \frac{4\pi}{k_{01}^2}\left\langle\varphi_2^{s(-)}(\mathbf{k}_2,R_\Omega\mathbf{r})\right|\left(e^{i\mathbf{k}_{01}\cdot\mathbf{r}} - \frac{\sum_n Z_n e^{i\mathbf{k}_{01}\cdot\mathbf{R}_n}}{\sum_n Z_n}\right) \\ &\quad \times\left|\varphi_i^s(R_\Omega\mathbf{r})\right\rangle \\ &\simeq \frac{4\pi}{k_{01}^2}\left\langle\varphi_2^{s(-)}(\mathbf{k}_2,R_\Omega\mathbf{r})\right|(e^{i\mathbf{k}_{01}\cdot\mathbf{r}} - 1)\left|\varphi_i^s(R_\Omega\mathbf{r})\right\rangle, \end{aligned} \tag{4}$$

where $\mathbf{k}_{01} = \mathbf{k}_0 - \mathbf{k}_1$ is the momentum transfer vector and $\varphi_i^s(\mathbf{r})$ and $\varphi_2^{s(-)}(\mathbf{k}_2,\mathbf{r})$ are the wave function of the ionized molecular orbital s (or Dyson orbital s) and the continuum wave function of the ejected electron from orbital s, respectively. Note that the last equation of (4) is approximately achieved by considering the fact that the nuclei are localized in a small region; however, the effect from the nuclei could eventually be taken into account in the present theoretical model. The first and second terms in Eq. (4) represent the scattering of the incoming electron by the ejected electron and the residual ion, respectively. The latter reduces to a Coulomb tail considering the localization of the nuclei [26]. We also note that most of the present distorted-wave (DW) methods are based on the single-active-electron approximation and then $\varphi_i^s(\mathbf{r})$ and $\varphi_2^{s(-)}(\mathbf{k}_2,\mathbf{r})$ will be orthogonal and only the first term in Eq. (4) contributes to the transition matrix. However, the orthogonality between $\varphi_i^s(\mathbf{r})$ and $\varphi_2^{s(-)}(\mathbf{k}_2,\mathbf{r})$ cannot be achieved if the continuum wave function $\varphi_2^{s(-)}(\mathbf{k}_2,\mathbf{r})$ is calculated with the spherically averaged potential for the molecular system. The previous DWBA calculations [26,31] show that the numerical results depend on the consideration of the second term of Eq. (4) or the Coulomb tail. The effect of the Coulomb tail is also studied by the present MCDW. The evaluation of the transition matrix of Eq. (4) can be simplified in the molecular frame as

$$T_{if}^s(\Omega) = \frac{4\pi}{k_{01}^2}\left\langle\varphi_2^{s(-)}\left(R_\Omega^{-1}\mathbf{k}_2,\mathbf{r}\right)\right|\left(e^{iR_\Omega^{-1}\mathbf{k}_{01}\cdot\mathbf{r}} - 1\right)\left|\varphi_i^s(\mathbf{r})\right\rangle, \tag{5}$$

where R_Ω^{-1} is the inverse operator of R_Ω. In the molecular frame, Eq. (5) can simply be understood as rotating the momentum vectors but fixing their relative geometries, where

$\mathbf{k}_2$ and $\mathbf{k}_{01}$ should be considered as the initial vectors given in the laboratory frame. Once the transition matrix and 8DCS for a specific molecular orientation are evaluated, the total fivefold differential cross section (5DCS) or the generally named TDCS can be obtained by geometry averaging as [29]

$$\frac{d^5\sigma}{d\Omega_2 d\Omega_1 dE_1} = \frac{1}{(2\pi)^5}\frac{k_1 k_2}{k_0}\frac{1}{8\pi^2}\int d\Omega \sum_{av} |T_{fi}(\Omega)|^2 \rho_R(\Omega), \tag{6}$$

where $\rho_R(\Omega)$ denotes the density distribution of the rotational wave packet. For the rotationally isotopic target, $\rho_R(\Omega) = 1$. Generally, there is no analytical way to simplify the geometry averaging or integration in Eq. (6). The 5DCS can be obtained by averaging the 8DCS for a series of different orientations. In the implementation, the Euler angles α, β, and γ are discrete with the Gauss-Legendre integral method, the 8DCS are calculated for all the discrete Euler angles or orientations, and the 5DCS is numerically achieved by summing all the 8DCS weighted by the Gaussian weights. Convergence should be checked by increasing the discrete points of the Euler angles.

Note that the above formalism is general within the molecular frozen-core approximation and the fast-electron plane-wave Born approximation. The main differences among different theories are the approaches to treat the slow ejected electron. The present multicenter distorted-wave method will be presented in the following section.

B. Multicenter distorted wave [8]

The wave function of the ejected electron could be obtained by solving the Schrödinger equation with the distorted or model potential $\mathbf{V}^m = \mathbf{V}^{st} + \mathbf{V}^{cp} + \mathbf{V}^{\text{model exc}}$, where $\mathbf{V}^{st}$, $\mathbf{V}^{cp}$, and $\mathbf{V}^{\text{model exc}}$ are the static, polarization, and model exchange potentials, respectively [48]. Note that these potentials are anisotropic and possess angular distributions. Different methods can be used to model the polarization potential [49,50] and the model exchange potential [51–54]. The latter also depends on the kinetic energy of the ejected electron. The correlation polarization potential based on the density-functional theory [49,55] and the modified semiclassical exchange potential [52,53,55] are used in the present work. The well-known static potential $\mathbf{V}^{st}$ also possesses the multicenter nature, explicitly,

$$\begin{aligned}\mathbf{V}^{st}(\mathbf{r}) &= \mathbf{V}^{ee}(\mathbf{r}) + \mathbf{V}^{en}(\mathbf{r}) \\ &= \int \rho(\mathbf{s})\frac{1}{|\mathbf{r}-\mathbf{s}|}d\mathbf{s} - \sum_n \frac{Z_n}{|\mathbf{r}-\mathbf{R}_n|},\end{aligned} \tag{7}$$

where $\rho(\mathbf{s})$ indicates the total electron density distributions of the ionic molecule and when r is large, $\mathbf{V}^{st}$ reduces to the Coulomb potential $-1/r$.

To avoid the difficulties in solving the three-dimensional potential, the conventional DW methods [7,29,32–36,46] employ the spherical averaging approximation to reduce the anisotropic potential to the r-dependent-only scalar or isotropic potential, as

$$\tilde{V}^m(k_2,r) = \frac{1}{4\pi}\int \mathbf{V}^m(k_2,\mathbf{r})d\hat{\mathbf{r}}.$$

For example, $\mathbf{V}^{en}(\mathbf{r})$ becomes

$$\tilde{V}^{en}(r) = -\sum_n \frac{Z_n}{R_n^>}, \tag{8}$$

where $R_n^> = \max\{r, R_n\}$. We comment that a great deal of important information would be lost by spherical averaging, especially the important angular-dependent multicenter nature of the potentials, since in Eq. (8) the potential only depends on the molecular bond length. The molecular anisotropic structure information is totally lost. We develop a multicenter distorted-wave method by exactly solving the three-dimensional potentials by employing the single-center expansion (SCE) techniques [48,55–58].

Generally speaking, any type of angular basis set, e.g., spherical harmonics $Y_{lm}(\theta,\varphi)$, can be used to expand the wave function and potential. Bearing in mind that a molecule possesses point group symmetry in the molecular frame, the symmetry-adapted angular function $X_{hl}^{pu}(\theta,\varphi)$ [55,58] would be the prior choice and is employed in this work, where p and u label one of the relevant irreducible representations and one of its components, respectively. Index h labels a specific basis, at a given angular momentum l, for the pth irreducible representations considered [55]. The symmetry-adapted angular function can be transformed from the spherical harmonics with the symmetry-dependent transformation matrix [55]. The total model potential can thus be expanded in the center of mass in terms of the symmetry-adapted angular functions belonging to the A_1 irreducible representations as [55]

$$\mathbf{V}^m(k_2,\mathbf{r}) = \sum_{lm} V_{lm}^m(k_2,r) X_{lm}^{A_1}(\theta,\varphi), \tag{9}$$

where $V_{lm}^m(k_2,r)$ is the radial part of the total model potential for a given (l,m) pair. The expansion of Eq. (9) can be performed using the published library SCELIB [55–57].

The wave function of the ejected electron $\phi_2^{s(-)}(\mathbf{k}_2,\mathbf{r})$ is obtained with the partial-wave-expansion method as

$$\begin{aligned}\left\langle \phi_2^{s(-)}(\mathbf{k}_2)\middle|\mathbf{r}\right\rangle &= 4\pi \sum_{l'm'}\sum_{lm} i^{-l'} e^{i\delta_{l'}^c}\frac{f_{l'l}(k_2,r)}{k_2 r} Y_{l'm'}^*(\hat{\mathbf{k}}_2) Y_{lm}(\hat{\mathbf{r}}) \\ &= \sum_{pu} 4\pi \sum_{h'l'}\sum_{hl} i^{-l'} e^{i\delta_{h'l'}^c}\frac{f_{h'l',hl}^{pu}(k_2,r)}{k_2 r} \\ &\quad \times X_{h'l'}^{pu}(\hat{\mathbf{k}}_2) X_{hl}^{pu}(\hat{\mathbf{r}}),\end{aligned} \tag{10}$$

where $\delta_{l'}^c = \delta_{h'l'}^c = \arg\Gamma(l'+1+i\eta)$ is the Coulomb phase shift. The summation for l' and m' or h' and l' in Eq. (10) are used to consider the coupling for different channels or the anisotropic property of the model potential in Eq. (9).

The coupled equations can be obtained by substituting Eq. (10) into the scattering equation:

$$\begin{aligned}&\left[\frac{d^2}{dr^2} - \frac{l(l+1)}{r^2} + k_2^2 + \frac{2}{r}\right] f_{h'l',hl}^{pu}(k_2,r) \\ &\quad = \sum_{h''l''} U_{h'l',h''l''}^{pu}(k_2,r) f_{h''l'',hl}^{pu}(k_2,r),\end{aligned} \tag{11}$$

where the potential matrix element is

$$U_{h'l',h''l''}^{pu}(k_2,r) = 2\left\langle X_{h'l'}^{pu}(\hat{\mathbf{r}})\middle|\mathbf{V}^m(k_2,\mathbf{r})\middle|X_{h''l''}^{pu}(\hat{\mathbf{r}})\right\rangle + \frac{2}{r}\delta_{h'h''}\delta_{l'l''}. \tag{12}$$

The coupled equations can further be rewritten in an integral form or Volterra equation [59] with the standard Green's-function technique as [48]

$$f^{pu}_{h'l',hl}(k_2,r) = \delta_{hh''}\delta_{ll''}F_l(k_2r) + \sum_{h''l''}\int_0^r dr' g_l(k_2,r,r')U_{hl,h''l''}(k_2,r')f^{pu}_{h''l'',hl}(k_2,r'), \tag{13}$$

where the Green's function

$$g_l(k_2,r,r') = \frac{1}{k_2}[F_l(k_2r)G_l(k_2r') - G_l(k_2r)F_l(k_2r')],$$

with F_l and G_l the regular and irregular Coulomb functions, respectively. The set of solutions of Eq. (13) can easily be solved with the numerical methods introduced in Ref. [59]. However, the physical wave function of Eq. (10) can only be obtained by matching the wave function with the physical asymptotic conditions [60], i.e.,

$$f^{pu}_{h'l',hl}(r) \underset{r\to\infty}{=} F_{h'l'}(k_2r) + H^{-}_{h'l'}(k_2r)T^{pu}_{h'l',hl} \underset{r\to\infty}{=} \sin\left(\theta^b_{h'l'} + \delta^c_{h'l'}\right)\delta_{h'l',hl} + e^{-i(\theta^b_{h'l'}+\delta^c_{h'l'})}T^{pu}_{h'l',hl}, \tag{14}$$

where $H^{-}_{h'l'}(k_2r)$ is the incoming Coulomb function, $\theta^b_{h'l'} = k_2r - l'\pi/2 - \eta\ln(2k_2r)$, with $\eta = 1/k_2$, and $\delta^c_{h'l'}$ is the Coulomb phase shift.

C. Transition matrix for a specific orientation

Similarly, the wave function $\phi^s_i(\mathbf{r})$ of the ionized orbital s is also expanded in the center of mass with the symmetry-adapted angular function as

$$\phi_s(\mathbf{r}) = r^{-1}\sum_{hl} u^s_{hl}(r)X^{p_su_s}_{hl}(\theta,\varphi). \tag{15}$$

The transition matrix for a specific orientation Ω is evaluated as

$$\begin{aligned} T^s_{if}(\Omega) &= \frac{4\pi}{k^2_{01}}\left\langle\varphi^{s(-)}_2\left(R^{-1}_\Omega\mathbf{k}_2,\mathbf{r}\right)\middle|\left(e^{iR^{-1}_\Omega\mathbf{k}_{01}\cdot\mathbf{r}}-1\right)\middle|\varphi^s_i(\mathbf{r})\right\rangle \\ &= \frac{4\pi}{k^2_{01}}\int r^2dr\int d\hat{\mathbf{r}}\sum_{pu}4\pi\sum_{h_1l_1h_2l_2} i^{-l_1}e^{i\delta^c_{h_1l_1}} \\ &\quad\times\frac{f^{pu}_{h_1l_1,h_2l_2}(k_2,r)}{k_2r}X^{pu}_{h_1l_1}\left(R^{-1}_\Omega\hat{\mathbf{k}}_2\right)X^{pu}_{h_2l_2}(\hat{\mathbf{r}}) \\ &\quad\times\left[4\pi\sum_{l_4m_4} i^{l_4}j_{l_4}(k_{01}r)S_{l_4m_4}\left(R^{-1}_\Omega\hat{\mathbf{k}}_{01}\right)S_{l_4m_4}(\hat{\mathbf{r}}) - 1\right] \\ &\quad\times r^{-1}\sum_{h_3l_3}u^s_{h_3l_3}(r)X^{p_su_s}_{h_3l_3}(\hat{\mathbf{r}}), \end{aligned} \tag{16}$$

where $j_l(kr)$ is the spherical Bessel function and $S_{lm}(\hat{\mathbf{r}})$ is the real spherical harmonics [55,61]. Equation (16) could be further simplified as

$$\begin{aligned} T^s_{if}(\Omega) &= \frac{(4\pi)^2}{k^2_{01}k_2}\sum_{pu}\sum_{h_1l_1h_2l_2} i^{-l_1}e^{i\delta^c_{h_1l_1}}X^{pu}_{h_1l_1}\left(R^{-1}_\Omega\hat{\mathbf{k}}_2\right) \\ &\quad\times\left[4\pi\sum_{l_4m_4} i^{l_4}S_{l_4m_4}\left(R^{-1}_\Omega\hat{\mathbf{k}}^i_{01}\right)A^{pu,p_su_s}_{l_4m_4,h_2l_2,h_3l_3}\right. \\ &\quad\left.\times\sum_{h_3l_3}B^{pu}_{h_1l_1,h_2l_2,h_3l_3,l_4} - \delta_{h_2h_3}\delta_{l_2l_3}\delta_{pp_s}\delta_{uu_s}C^{pu}_{h_1l_1,h_2l_2,h_3l_3}\right], \end{aligned} \tag{17}$$

where A, B, and C are defined as

$$\begin{aligned} A^{pu,p_su_s}_{l_4m_4,h_2l_2,h_3l_3} &= \int d\hat{\mathbf{r}}\, S_{l_4m_4}(\hat{\mathbf{r}})X^{pu}_{h_2l_2}(\hat{\mathbf{r}})X^{p_su_s}_{h_3l_3}(\hat{\mathbf{r}}), \\ B^{pu}_{h_1l_1,h_2l_2,h_3l_3,l_4} &= \int dr\, f^{pu}_{h_1l_1,h_2l_2}(k_2,r)j_{l_4}(k_{01}r)u^s_{h_3l_3}(r), \\ C^{pu}_{h_1l_1,h_2l_2,h_3l_3} &= \int dr\, f^{pu}_{h_1l_1,h_2l_2}(k_2,r)u^s_{h_3l_3}(r). \end{aligned} \tag{18}$$

The 8DCS and TDCS can be calculated with relations (1) and (6), respectively. The application of the present multicenter distorted-wave method and the numerical results are shown in the next section.

III. RESULTS AND DISCUSSION

H_2O has been extensively studied by both theoretical and experimental works [26,28,30,31] in the coplanar-asymmetric kinematics, which serves as a good case to test the present multicenter distorted-wave method. H_2O belongs to C_{2V} symmetry and its ground-state electronic configuration is $1a_1^2 2a_1^2 1b_2^2 3a_1^2 1b_1^2$ with bond length $R_{O-H} = 1.81$ a.u. and bond angle $\angle_{H-O-H} = 104.5°$. In the calculation, all the molecular orbitals (MOs) are first prepared within the Hartree-Fock level as HF/cc-pVTZ (6D 10F) with GAUSSIAN 03 [62]. Then the MOs are expanded into the center of mass with the symmetry-adapted angular functions as Eq. (15). Note that in the present case (C_{2V}), the symmetry-adapted angular functions can be reduced to the well-known real-spherical harmonics $S_{lm}(\hat{\mathbf{r}})$ [61] explicitly. The angular basis for MOs a_1, b_1, and b_2 satisfies the conditions $m = 0,2,4,\ldots$, $m = 1,3,\ldots$, and $m = -1,-3,\ldots$, respectively. In the SCE, the r space is discrete from 0 to 8.5 a.u. by a gradually increasing mesh grid with step size from 0.001 to 0.128 a.u. The convergence of the SCE is easily reached in the present case when l is larger than 6. However, the maximum l is chosen to be 25 to make sure the convergence of the partial-wave expansion for the slow electron. The radial parts of the SCE MOs $1b_1$, $3a_1$, $1b_2$, and $2a_1$ are shown in Fig. 1 for the first few l. It is interesting to observe that all the MOs $1b_1$, $3a_1$, $1b_2$, and $2a_1$ are dominated by only one component $S_{1,1}$, $S_{1,0}$, $S_{1,-1}$, and $S_{0,0}$, respectively, with more than 97%, 91%, 96%, and 94% of the total charges in each orbital. The MOs $1b_1$, $3a_1$, and $1b_2$ and MO $2a_1$ look like the atomic p-type and s-type orbitals, respectively, which would result in quite

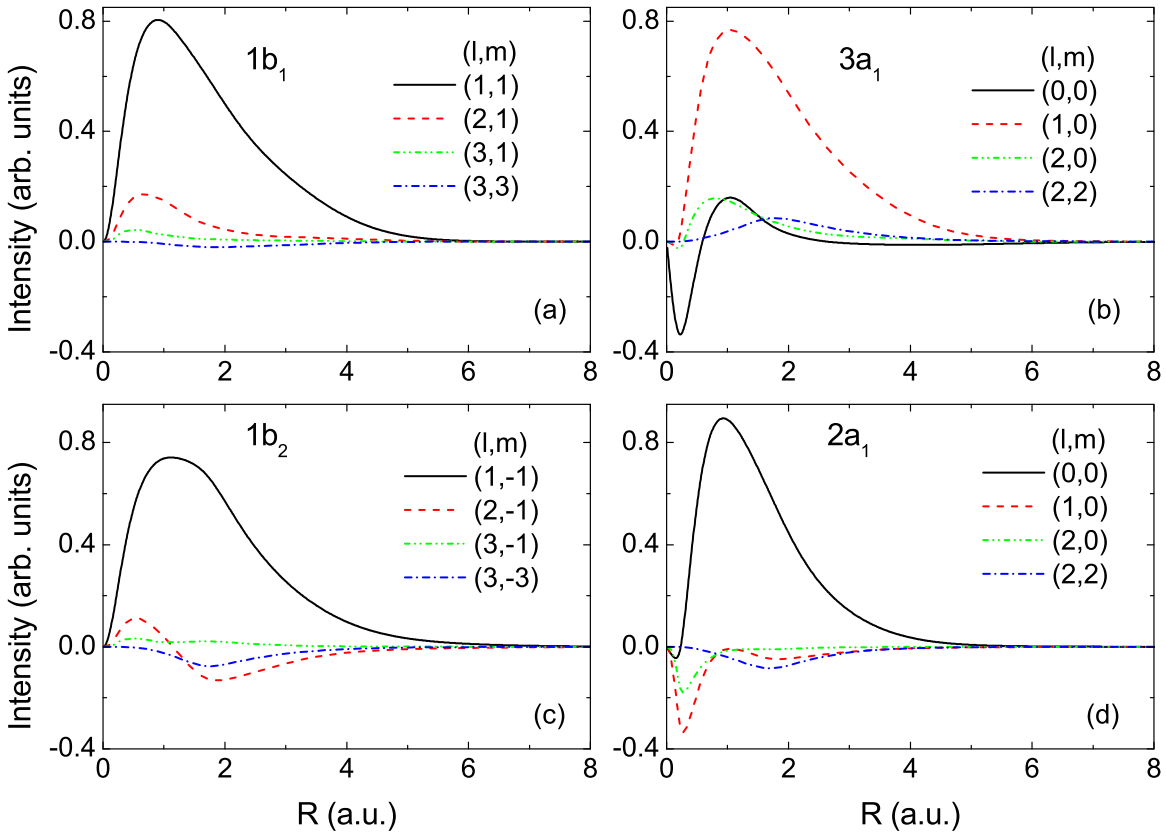

FIG. 1. (Color online) Radial parts of the center-of-mass expanded molecular orbitals $1b_1$, $3a_1$, $1b_2$, and $2a_1$. Here (l,m) indicates the angular component $S_{lm}(\hat{\mathbf{r}})$.

different dynamic patterns for the differential cross section (DCS). The one-component-dominated feature of the MOs is consistent with the fact that oxygen is the only heavy nucleus in a water molecule and the molecular system with only one heavy nucleus has been studied with the one-center basis-set self-consistent field (SCF) by Moccia [63–65].

The TDCS or 5DCS for the present calculations, the experimental measurements, and other theoretical results with the experimental scattering parameters [31] are shown in Fig. 2. The incident electron energy E_0 is 250 eV, the ejected electron energy E_2 is 10 eV (8 eV if the electron is ionized from orbital $3a_1$), and the scattering angle φ_1 is fixed at 15° [31]. The experimental and DWBA results are normalized to the main forward peak or binary peak of each orbital of the present MCDW results [the second and first forward peaks for Figs. 2(a)–2(d) and 2(e), respectively]. As the figure shows, the forward TDCS for orbitals $1b_1$, $3a_1$, $1b_2$, and $2a_1$ is dominated by two peaks at around 40° and 100° and one peak at around 60°, which is directly related to the orbital natures of p and s types [66,67], respectively. The present MCDW method better describes these forward patterns than the conventional DWBA [26]. Interestingly, the present MCDW method also predicts a second forward peak for $2a_1$ at around 140° and obviously more precise measurements are required to justify the existence of this binary peak. There are more uncertainties about the structures for the backward TDCS [recoil peak(s)]. The DWBA predicts one big (or one small) backward peak, while the present MCDW method predicts double-shoulder structures (or one big peak) for the backward scattering for the p-like orbitals $1b_1$, $3a_1$, and $1b_2$ (or s-like orbital $2a_1$). The present MCDW method also well reproduces the dominant backward peak for orbital $2a_1$ at around 240° (a second weaker peak is also predicted at around 350°). The uncertainties are large for the available experimental TDCS for backward scattering. It is difficult to identify the structures for orbitals $1b_1$, $3a_1$, and $1b_2$ and hence more precise measurements are required.

The results for different theories without the Coulomb tail are also shown in Fig. 2 for comparison. It shows that the DWBA without a Coulomb tail [31] can well reproduce the forward peak(s), but predicts no backward structures for the TDCS. Furthermore, the present MCDW method without a Coulomb tail basically produces results similar to those of the present MCDW method, which results from the fact that the model potential employed to calculate the continuum wave function for the ejected electron is very similar to the SCF potential for the ionized bound orbital and no further spherical averaging approximation is applied for the model potential when calculating the continuum wave function [see the text below Eq. (4) for further description]. These results also reveal the importance of solving the anisotropic distorted potential. Note that Ref. [26] also shows that the Coulomb wave Born approximation (CWBA) and the DWBA (with or without a Coulomb tail) predict very similar TDCS results, together with the TDCS results from the present MCDW method. We may learn that for a fixed molecular orbital with the present scattering kinematics, the forward peaks of the TDCS are more

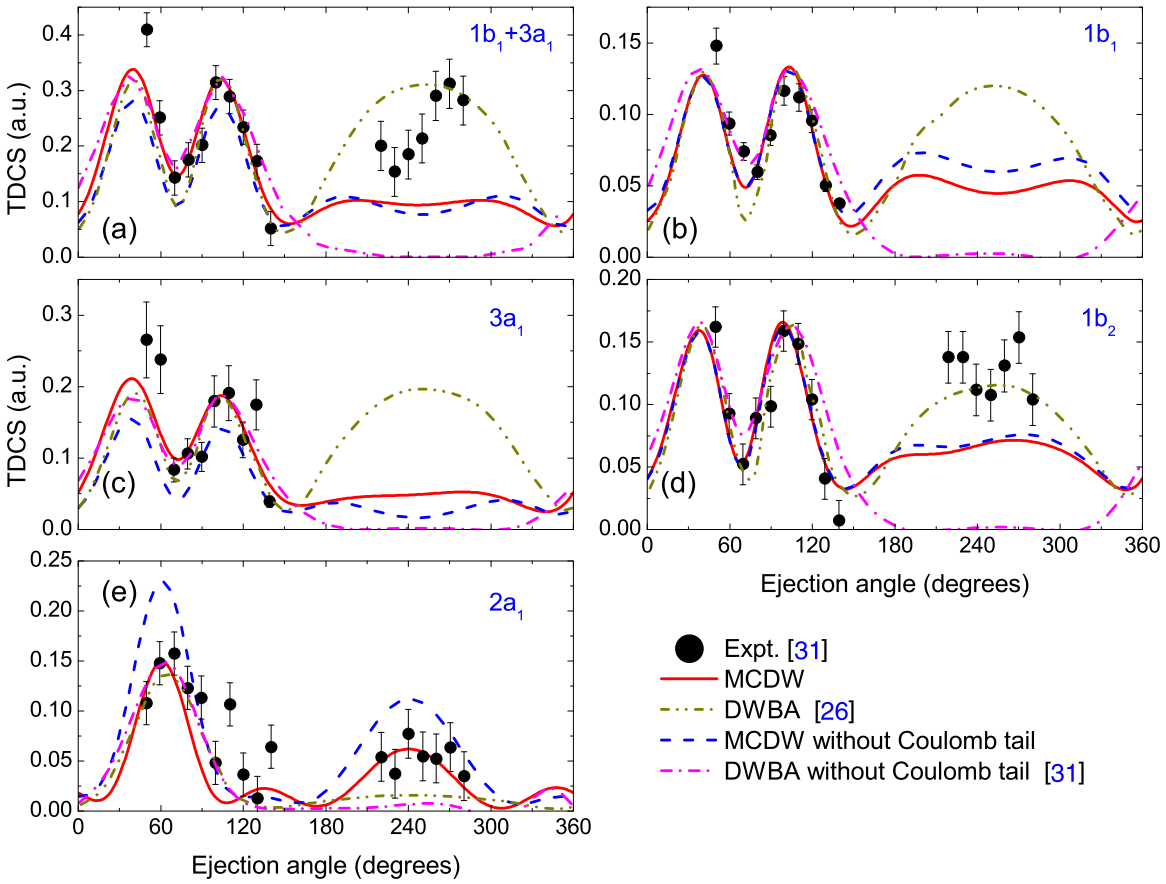

FIG. 2. (Color online) The TDCS for the present calculations and experimental measurements and other theoretical results with the same scattering parameters: The incident electron energy E_0 is 250 eV, the ejected electron energy E_2 is 10 eV (8 eV if the electron is ionized from orbital $3a_1$), and the scattering angle is 15°. The experimental and DWBA results are normalized to the main forwarding peak of each orbital of the present results (the second and first forward peaks in (a)–(d) and (e), respectively).

related to the pure electron-electron interactions between the scattering electron and ejected electron; the exact behavior of the continuum wave function for the small-r region is not so important. However, the backward structures of the TDCS are dominated by the continuum wave function and the accuracy of the continuum wave function in the small-r region greatly affects the final calculation results.

More interesting information can be obtained from the orientation-dependent DCS or 8DCS. The scattering kinematics and the initial molecular orientation of H_2O are defined in Fig. 3, where the x-y plane is chosen as the scattering plane. An oxygen atom lies in the positive-z axis, while hydrogen atoms lie in the y-z plane but below the scattering plane. The angles φ_1 and φ_2 are defined as the angles with respect to the incoming vector or x axis for the scattered and ejected electrons, respectively. Here we present the 8DCS for two different molecular orientations, the initial one $\Omega_1 = (0,0,0)$ and the second one $\Omega_2 = (0,0,90^\circ)$. The energies for the incident and the ejected electrons are 250 and 10 eV, respectively. Figure 4 shows the 8DCS results of the CWBA (with a Coulomb tail), the CWBA without a Coulomb tail, and the MCDW method for orbitals $1b_1$ and $2a_1$ with scattering angles 0° and 15°. As shown, 8DCS displays complex dynamic structures for different scattering parameters and different molecular orientations. It is interesting to observe that the CWBA and the MCDW method predict similar structures for orbitals $1b_1$ and quite different structures for orbitals $2a_1$ for the same scattering parameters. This would imply that the continuum

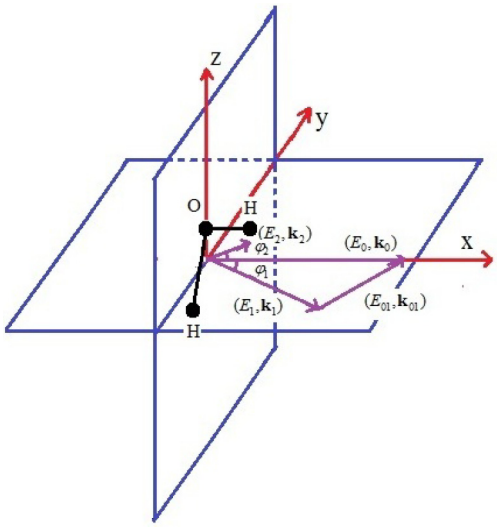

FIG. 3. (Color online) Illustration of the initial molecular orientation of H_2O and the coplanar-asymmetric kinematics. The molecule is in the y-z plane and the scattering is in the x-y plane.

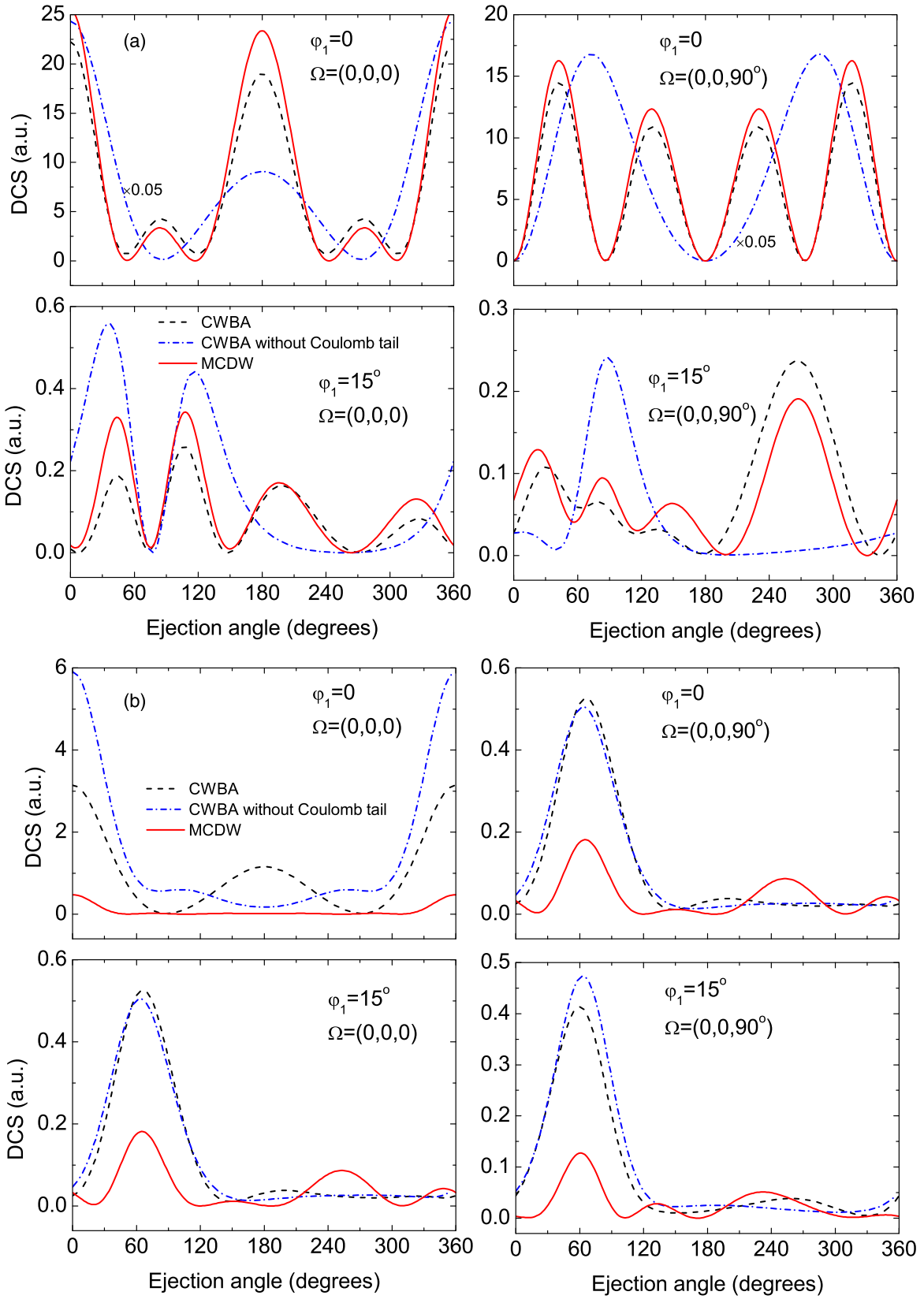

FIG. 4. (Color online) The 8DCS from the CWBA (with Coulomb tail) and CWBA without a Coulomb tail and MCDW for molecular orientations $\Omega_1 = (0,0,0)$ and $\Omega_2 = (0,0,90^\circ)$ for scattering angles of 0° and 15° for orbitals (a) $1b_1$ and (b) $2a_1$. The incident electron energy E_0 is 250 eV and the ejected electron energy E_2 is 10 eV.

electron ejected from the HOMO $1b_1$ does not experience much distortion compared with the pure Coulomb potential, but the continuum electron ejected from the inner valence $2a_1$ interacts with the residual target more strongly, which experiences a big distortion from the pure Coulomb potential in the small-r region. When the scattering angle $\varphi_1 = 0°$, the momentum transfer vector is along the x axis or the incident vector, the 8DCS could partly reflect the spatial charge distributions of the molecular orbitals [8,28], especially for orbital $1b_1$. When the scattering angle is increased to 15°, the dynamic structures are highlighted or downplayed by the electron-electron interactions. It is interesting to point out that the 8DCS for orbital $2a_1$ possesses structures similar to its TDCS when $\varphi_1 = 15°$, which could be related to its s-like orbital nature. It is also interesting to note that for the two chosen orientations, when $\varphi_1 = 0°$, the CWBA without a Coulomb tail predicts quite different structures from the other two models for orbital $1b_1$. When $\varphi_1 = 15°$, the CWBA without a Coulomb tail predicts the main binary peaks, but no recoil structures, for orbitals $1b_1$ and $2a_1$. We also note that there is a nodal plane for orbital $1b_1$ (also for orbitals $3a_1$ and $1b_2$), the scattering would be exactly in the nodal plane when $\Omega = (\alpha,90^\circ,0)$ (α is any angle), and no ionization would happen at those orientations for orbital $1b_1$, which is supported by our calculations but different from the predictions of Ref. [28].

It could be concluded that the present MCDW method has been successfully applied to study the $(e, 2e)$ dynamics of H_2O. However, more precise measurements are required to further check the present method because even for the TDCS data of the H_2O molecule, there are no consistent conclusions for the structures of the recoil peaks for the first three orbitals. Recently, the complex Kohn approach (CKA) was developed for the study of fast-electron-impact single ionization of molecules [68]. The CKA is also applied to the water molecule. The main results (the structure of the TDCS) of the CKA (Fig. 2 of Ref. [68]) are very similar to those of the present MCDW method (Fig. 2). Note that the CKA and MCDW method are at the same level by using a single-configuration SCF target, but the CKA would be more advanced by including the effect of coupled channels.

IV. CONCLUSION

We presented a universal and inexpensive multicenter distorted-wave method for electron-impact single ionization of a molecular system in the coplanar-asymmetric kinematics. Within this method, the fast incoming and outgoing electrons are described by the plane waves, while the slow ejected electron is described by the multicenter distorted wave, which is solved from the anisotropic multicenter potential between the ejected electron and the ionic molecule. Note that the MCDW method improves the conventional molecular distorted-wave methods, whose distorted wave is solved from the spherically averaged isotropic potential. The water molecule, with relatively good available experimental data, is chosen and studied with the present MCDW method. A comparison shows that the present MCDW method not only describes well the forward or binary structures, but also reasonably predicts the backward or recoil structures of the TDCS for all the molecular orbitals.

ACKNOWLEDGMENTS

S.B and X.Y. thanks for Dr. Gao Xiang for helpful discussions. This work was partly supported by the National Basic Research Program of China (Grants No. 2010CB923301 and No. 2013CB922200), the National Natural Science Foundation of China (Grants No. 11327404, No. 10734040 and No. 11025417) and NSAF of China (Grant No. U1330117).

[1] I. E. McCarthy and E. Weigold, Phys. Rep. **27**, 275 (1976).
[2] I. E. McCarthy and E. Weigold, Rep. Prog. Phys. **51**, 299 (1988).
[3] F. W. Byron, Jr. and C. J. Joachain, Phys. Rep. **179**, 211 (1989).
[4] I. E. McCarthy and E. Weigold, Rep. Prog. Phys. **54**, 789 (1991).
[5] M. A. Coplan, J. H. Moore, and J. P. Doering, Rev. Mod. Phys. **66**, 985 (1994).
[6] E. Weigold and I. E. McCarthy, *Electron Momentum Spectroscopy* (Kluwer Academic, New York, 1999).
[7] D. H. Madison and O. Al-Hagan, J. At. Mol. Opt. Phys. **2010**, 367180 (2010).
[8] There is no precise or strict definition for the fast or slow electrons. However, the general or default rules in the conventional electron-scattering process are applied in the present work, i.e., the free electrons with kinetic energies at the order of the ionization potential or much bigger than the ionization potential would be considered slow or fast electrons, respectively, and the Born approximation could be also applied to the fast electrons. See also S. B. Zhang, Ph.D. thesis, University of Science and Technology of China, 2011.
[9] I. McCarthy, Aust. J. Phys. **48**, 1 (1995).
[10] I. McCarthy and E. Weigold, *Electron Atom Collisions* (Cambridge University Press, Cambridge, 1995).
[11] D. H. Madison, R. V. Calhoun, and W. N. Shelton, Phys. Rev. A **16**, 552 (1977).
[12] M. Brauner, J. S. Briggs, and H. Klar, J. Phys. B **22**, 2265 (1989).
[13] J. Berakdar, Phys. Rev. A **53**, 2314 (1996).
[14] Z. Chen, Q. Shi, S. Zhang, J. Chen, and K. Xu, Phys. Rev. A **56**, R2514(R) (1997).
[15] O. Zatsarinny and K. Bartschat, Phys. Rev. Lett. **107**, 023203 (2011).
[16] O. Zatsarinny and K. Bartschat, J. Phys. B **47**, 061001 (2014).
[17] I. Bray and A. T. Stelbovics, Phys. Rev. A **46**, 6995 (1992).
[18] I. Bray and D. V. Fursa, Phys. Rev. A **54**, 2991 (1996).
[19] I. Bray, V. F. Dmitry, J. Röder, and H. Ehrhardt, J. Phys. B **30**, L101 (1997).
[20] C. W. McCurdy and T. N. Rescigno, Phys. Rev. A **56**, R4369 (1997).
[21] T. N. Rescigno, M. Baertschy, D. Byrum, and C. W. McCurdy, Phys. Rev. A **55**, 4253 (1997).
[22] T. N. Rescigno, M. Baertschy, W. A. Isaacs, and C. W. McCurdy, Science **286**, 2474 (1999).

[23] M. S. Pindzola and F. Robicheaux, Phys. Rev. A **54**, 2142 (1996).
[24] M. S. Pindzola and D. R. Schultz, Phys. Rev. A **53**, 1525 (1996).
[25] M. S. Pindzola, F. Robicheaux, S. D. Loch, J. C. Berengut, T. Topcu, J. Colgan, M. Foster, D. C. Griffin, C. P. Ballance, D. R. Schultz *et al.*, J. Phys. B **40**, R39 (2007).
[26] C. Champion, C. Dal Cappello, S. Houamer, and A. Mansouri, Phys. Rev. A **73**, 012717 (2006).
[27] C. Champion, J. Hanssen, and P.-A. Hervieux, J. Chem. Phys. **121**, 9423 (2004).
[28] C. Champion, J. Hanssen, and P. A. Hervieux, Phys. Rev. A **63**, 052720 (2001).
[29] C. Champion, J. Hanssen, and P. A. Hervieux, Phys. Rev. A **65**, 022710 (2002).
[30] C. Champion, J. Hanssen, and P. A. Hervieux, J. Chem. Phys. **117**, 197 (2002).
[31] D. S. Milne-Brownlie, S. J. Cavanagh, B. Lohmann, C. Champion, P. A. Hervieux, and J. Hanssen, Phys. Rev. A **69**, 032701 (2004).
[32] J. Gao, D. H. Madison, and J. L. Peacher, Phys. Rev. A **72**, 020701 (2005).
[33] J. Gao, D. H. Madison, and J. L. Peacher, Phys. Rev. A **72**, 032721 (2005).
[34] J. Gao, D. H. Madison, and J. L. Peacher, J. Chem. Phys. **123**, 204314 (2005).
[35] J. Gao, D. H. Madison, and J. L. Peacher, J. Phys. B **39**, 1275 (2006).
[36] J. Gao, D. H. Madison, J. L. Peacher, A. J. Murray, and M. J. Hussey, J. Chem. Phys. **124**, 194306 (2006).
[37] J. Gao, J. L. Peacher, and D. H. Madison, J. Chem. Phys. **123**, 204302 (2005).
[38] I. Tóth and L. Nagy, J. Phys. B **43**, 135204 (2010).
[39] S. Mohammed, B. Mammar, L. Boumediene, and D. Mevlüt, J. Phys. B **46**, 115206 (2013).
[40] J. Colgan, M. S. Pindzola, F. Robicheaux, C. Kaiser, A. J. Murray, and D. H. Madison, Phys. Rev. Lett. **101**, 233201 (2008).
[41] J. Colgan, O. Al-Hagan, D. H. Madison, C. Kaiser, A. J. Murray, and M. S. Pindzola, Phys. Rev. A **79**, 052704 (2009).
[42] M. S. Pindzola, F. Robicheaux, and J. Colgan, J. Phys. B **38**, L285 (2005).
[43] M. S. Pindzola, F. Robicheaux, S. D. Loch, and J. P. Colgan, Phys. Rev. A **73**, 052706 (2006).
[44] M. S. Pindzola, Sh. A. Abdel-Naby, J. A. Ludlow, F. Robicheaux, and J. Colgan, Phys. Rev. A **85**, 012704 (2012).
[45] M. C. Zammit, D. V. Fursa, and I. Bray, Phys. Rev. A **87**, 020701 (2013).
[46] H. Aouchiche, C. Champion, and D. Oubaziz, Radiat. Phys. Chem. **77**, 107 (2008).
[47] O. Al-Hagan, C. Kaiser, D. Madison, and A. J. Murray, Nat. Phys. **5**, 59 (2009).
[48] N. Sanna, I. Baccarelli, and G. Morelli, Comput. Phys. Commun. **180**, 2550 (2009).
[49] F. A. Gianturco, A. Jain, and J. A. Rodriguez-Ruiz, Phys. Rev. A **48**, 4321 (1993).
[50] J. K. O'Connell and N. F. Lane, Phys. Rev. A **27**, 1893 (1983).
[51] S. Hara, J. Phys. Soc. Jpn. **22**, 710 (1967).
[52] F. A. Gianturco and S. Scialla, J. Phys. B **20**, 3171 (1987).
[53] F. A. Gianturco, L. C. Pantano, and S. Scialla, Phys. Rev. A **36**, 557 (1987).
[54] J. B. Furness and I. E. McCarthy, J. Phys. B **6**, 2280 (1973).
[55] N. Sanna and F. A. Gianturco, Comput. Phys. Commun. **128**, 139 (2000).
[56] N. Sanna and G. Morelli, Comput. Phys. Commun. **162**, 51 (2004).
[57] N. Sanna, I. Baccarelli, and G. Morelli, Comput. Phys. Commun. **180**, 2544 (2009).
[58] F. A. Gianturco, D. G. Thompson, and A. K. Jain, in *Computational Methods for Electron Molecule Collisions*, edited by W. M. Huo and F. A. Gianturco (Plenum, New York, 1994).
[59] T. A. Burton, *Volterra Integral and Differential Equations*, 2nd ed. (Elsevier Science, Amsterdam, 2005).
[60] J. R. Taylor, *Scattering Theory: The Quantum Theory of Nonrelativistic Collisions* (Wiley, New York, 1972).
[61] H. H. H. Homeier and E. O. Steinborn, J. Mol. Struct. (Theochem) **368**, 31 (1996).
[62] M. J. Frisch, G. W. Trucks, H. B. Schlegel, G. E. Scuseria, M. A. Robb, J. R. Cheeseman, G. Scalmani, V. Barone, B. Mennucci, G. A. Petersson *et al.*, GAUSSIAN 03, Revision A.1 (2003).
[63] R. Moccia, J. Chem. Phys. **40**, 2186 (1964).
[64] R. Moccia, J. Chem. Phys. **40**, 2164 (1964).
[65] R. Moccia, J. Chem. Phys. **40**, 2176 (1964).
[66] L. Q. Chen, X. J. Chen, X. J. Wu, X. Shan, and K. Z. Xu, J. Phys. B **38**, 1371 (2005).
[67] L. Avaldi, R. Camilloni, R. Multari, G. Stefani, X. Zhang, H. R. J. Walters, and C. T. Whelan, Phys. Rev. A **48**, 1195 (1993).
[68] C.-Y. Lin, C. W. McCurdy, and T. N. Rescigno, Phys. Rev. A **89**, 012703 (2014).